EUROFUSION WPS1-PR(16) 15034

D Moseev et al.

Absolute calibration of sniffer probes on Wendelstein 7-X

Preprint of Paper to be submitted for publication in
Review of Scientific Instruments

This work has been carried out within the framework of the EUROfusion Consortium and has received funding from the Euratom research and training programme 2014-2018 under grant agreement No 633053. The views and opinions expressed herein do not necessarily reflect those of the European Commission.

Absolute calibration of sniffer probes on Wendelstein 7-X

D Moseev[1], H P Laqua[1], S Marsen[1], T Stange[1], H Braune[1], V Erckmann[1], F Gellert[1,2], J W Oosterbeek[3]

[1]Max-Planck-Institut für Plasmaphysik, Greifswald, Germany
[2]Ernst-Moritz-Arndt-Universität Greifswald, Greifswald, Germany
[3]Eindhoven University of Technology, Eindhoven, The Netherlands

E-mail: dmitry.moseev@ipp.mpg.de

Abstract.

Here we report the first measurements of the power levels of stray radiation in the vacuum vessel of Wendelstein 7-X using absolutely calibrated sniffer probes. The absolute calibration was achieved by using calibrated sources of stray radiation and implicit measurement of the quality factor of the Wendelstein 7-X empty vacuum vessel. Normalized absolute calibration coefficients agree well with the cross-calibration coefficients that were obtained by the direct measurements, indicating that the measured absolute calibration coefficients and stray radiation levels in the vessel are reliable. The stray radiation reaches power levels up to 340 kW/m^2 per MW injected beam power in close to the launcher. Most distant from the launcher, i.e. half a toroidal turn, still 80 kW/m^2 per MW injected beam power are measured.

24 February 2016

1. Introduction

Wendelstein 7-X is an optimized stellarator built of five identical modules [1]. Electron cyclotron resonance heating (ECRH) at 140 GHz is used as a main heating mechanism in the machine [1–4]. The ECRH system will deliver up to 10 MW of microwave power in continuous regime [2]. Even a small fraction of non-absorbed microwave radiation may damage diagnostics and machine components if they are not properly screened [5]. Stray radiation is a nuisance for microwave-based diagnostics. Accurate knowledge of the stray radiation energy flux is vital for proper protection of the Collective Thomson Scattering diagnostic which is installed or planed on many machines [6–9] and will be installed in Wendelstein 7-X in the next experimental campaign. Hence a set of diagnostics is installed in order to monitor and control the level of non-absorbed microwave power: sniffer probes, microwave bolometers [4], electron cyclotron absorption (ECA) diagnostic [10], (near) infrared video (IR) cameras [11].

Sniffer probes [12] belong to the standard set of diagnostics for machine safety and are for example installed in ASDEX Upgrade [13], LHD [14]. Typically interlocks are fed with the sniffer probe measurements and the threshold is determined experimentally. However, the steady-state operation requires more accurate knowledge on the distribution of stray radiation and, moreover, on the absolute values of the energy flux in the different parts of the machine.

In Section 2 the design and the arrangement of sniffer probes on Wendelstein 7-X is described. The absolute calibration of sniffer probes against modeling is explained in Section 3. Section 4 describes an independent cross-calibration procedure for the sniffer probes. The absolute calibration and cross-calibration are compared and combined into one calibration curve in Section 5. Section 6 concludes the paper.

2. Experimental setup

There are five sniffer probes in the Wendelstein 7-X stellarator. They are installed in ports AEB 11, 21, 31, 41, and 51 in modules 1, 2, 3, 4, and 5 respectively. Their location in the machine is displayed in Fig. 1. A sketch illustrating their design is shown in Fig. 2. On the right panel a front-end part of the diagnostic is shown: a water-cooled stainless steel shield which is necessary for high performance steady-state experiments. The back-end part consists of a copper tube acting as oversized waveguide. The microwaves pass through a copper tube and a vacuum window (fused silica) and are then focused by a concave teflon lens on a Schröder diffusor [15]. This assembly should ensure the wide angle antenna acceptance pattern. An attenuator is installed between the horn and the diode in order to prevent saturation of the amplifier and data acquisition system.

3. Absolute calibration of sniffer probes

The absolute calibration of sniffer probes was performed independently from the cross-calibration of the probes. Gyrotrons C1 (module 1) and D5 (module 5) were used as sources of stray radiation. The gyrotrons were not used simultaneously. The underlying principle of the absolute calibration is intrinsic estimation of the quality factor of the Wendelstein 7-X vacuum vessel using calibrated sources. One of the biggest problem of the method is large volatility in the sniffer probe signal. It is overcome by multiple averaging over:

- gyrotron frequency chirp,
- time,
- gyrotron polarization.

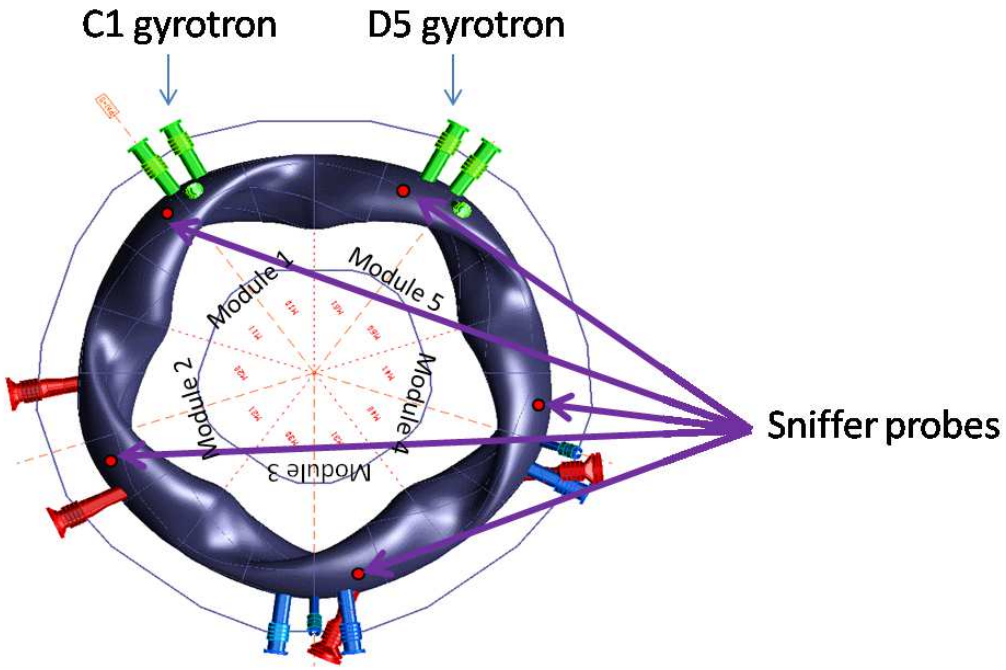

Figure 1. Sketch showing a top view of Wendelstein 7-X. Green ports at the top denote the location of the C1 and D5 launchers used as sources of stray radiation. Red circles show the location of ports AEB 11, 21, 31, 41, and 51 in modules 1-5 where the sniffer probes are installed.

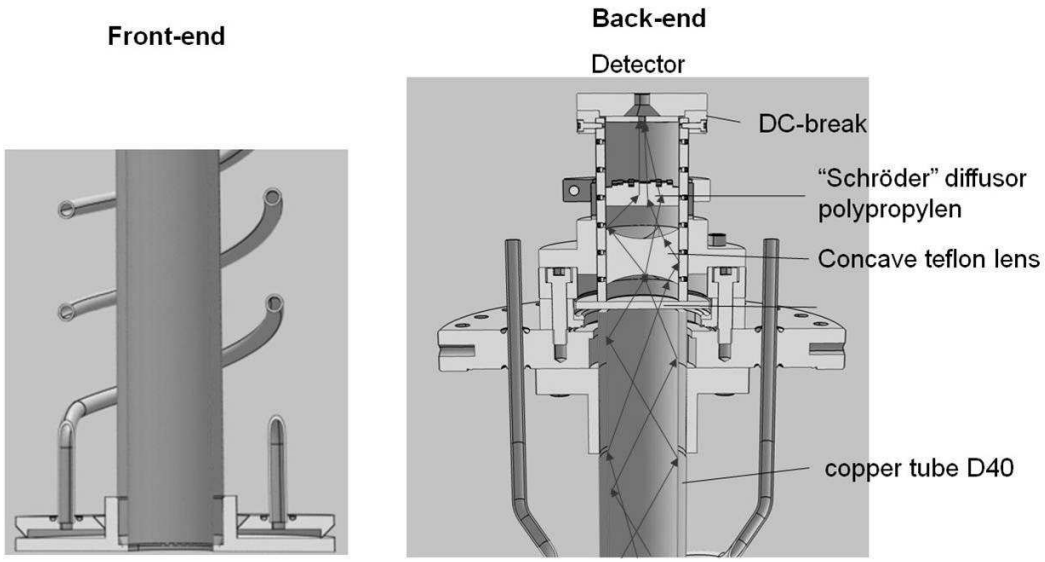

Figure 2. A sketch of the sniffer probe design for Wendelstein 7-X. Water-cooled stainless steel shield is mounted in the front-end part (left). The back-end part (on the right) has a copper-made oversized waveguide, a biconcave teflon lens, a Schröder diffusor, and a detection diode.

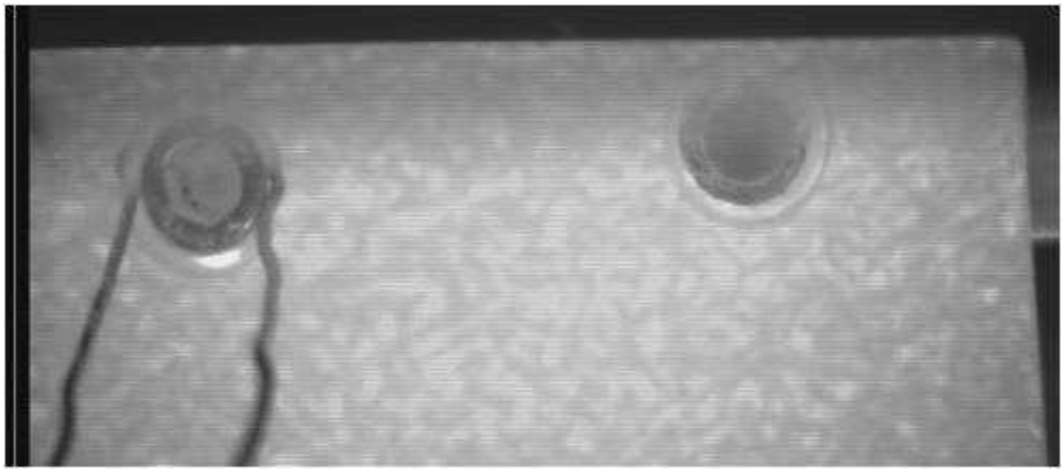

Figure 3. Snapshot from IR camera in the MISTRAL chamber, the flakes are showing the fine-grained heat distribution due to the interference pattern of the gyrotron radiation. The gyrotron pulse duration was 1 ms, and the picture was taken after the pulse. The exposure time was 5 ms.

3.1. Gyrotron modulation

Gyrotrons are sources of coherent high-power microwave radiation. We use gyrotrons as sources for the absolute calibration of the sniffer probes. As the radiation is coherent, strong interference patterns form in the vacuum vessel. Due to the frequency chirp of gyrotrons, the resulting interference pattern is not stationary. The strongly non-uniform heat distribution in the wall due to the interference pattern from the gyrotrons were observed by IR cameras during the experiments in the MISTRAL chamber [3]. Fig. 3 shows an IR picture with 5 ms exposure time was taken after a 1 ms long gyrotron pulse into the chamber. The thermal signature of the interference pattern of a mm-scale can be observed with such a short experimental timing as thermal transport due to heat conduction happens on a longer timescale and the gyrotron frequency chirp is not significant.

The existence of these interference patterns is a nuisance for sniffer probe calibration as the sniffer probe measurements will depend on the location in this interference pattern. For example, one could obtain very large signals for constructive interference and very low signals for destructive interference. During a plasma discharge, there will be no interference pattern since the plasma destroys the coherence of the radiation. Hence we need to minimize the impact of the interference pattern in the calibration experiments. Here we exploit that the gyrotron frequency changes when the power is modulated. We modulated the gyrotron power by 90%. The modulation frequency of the accelerating voltage in the range 66-78 kV was 10 kHz. This power modulation on this short time scale results in frequency chirps of about 30 MHz. The gyrotrons were modulated for 10 ms corresponding to 100 cycles.

One could argue that the frequency changes less than 1% and that it is not

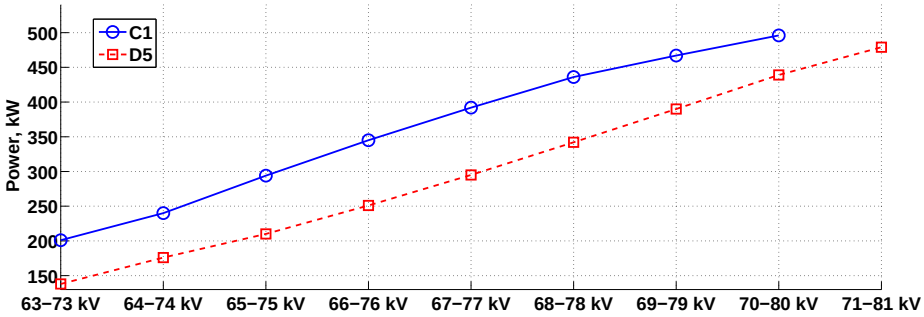

Figure 4. Calibration curves for the gyrotrons C1 and D5 in the modulation regime. Lower and upper values of the acceleration voltage are shown on X axis and corresponding average power is depicted on Y axis.

significant, however after numerous reflections the difference of optical paths of interfering waves can easily reach one wavelength. Sniffer probe amplifiers are equipped with low-pass filters with a cut-off frequency of 5 kHz. Therefore the signal on data acquisition cards is intrinsically averaged over the frequency chirp.

For quantitative analysis of the gyrotron stray radiation, the gyrotrons were calibrated in the modulated regime by calorimetry measurements. Steerable mirrors in the transmission lines for gyrotrons C1 and D5 [2] redirect microwaves into the water load instead of the vacuum vessel of the stellarator. Transmission losses are taken into account. The power-voltage curves of the gyrotrons are shown in Fig. 4. The upper and lower values of the accelerating voltage are shown on x-axis and the average power is shown on y-axis.

3.2. Averaging of the sniffer probe signals

The sniffer probes should provide absolute power levels of stray radiation during plasma discharges. Our calibration is, however, performed by launching the microwave beam into the empty vacuum vessel without plasma. In addition to the intrinsic frequency averaging due to the 5 kHz low-pass filter and power modulation, we average over the polarization of the injected microwave power by turning the polarizer plates. This has to be done as stray radiation in a plasma experiment is arbitrarily polarized whereas the injected microwave power in the calibration is polarized. We averaged over five different polarizer settings. The polarization vector of gyrotron radiation was changed from -90° to +90° with 45° steps.

Polarization averaging can be replaced by averaging over gyrotron launching directions, which has a similar effect. In the discussed experiments polarization averaging was performed using gyrotron C1 as a source; launching direction averaging was performed using gyrotron D5 as a source. The impact locations are shown in Fig. 8 by red circles. The beam impact positions are located in half-modules 51 and 50. This figure shows

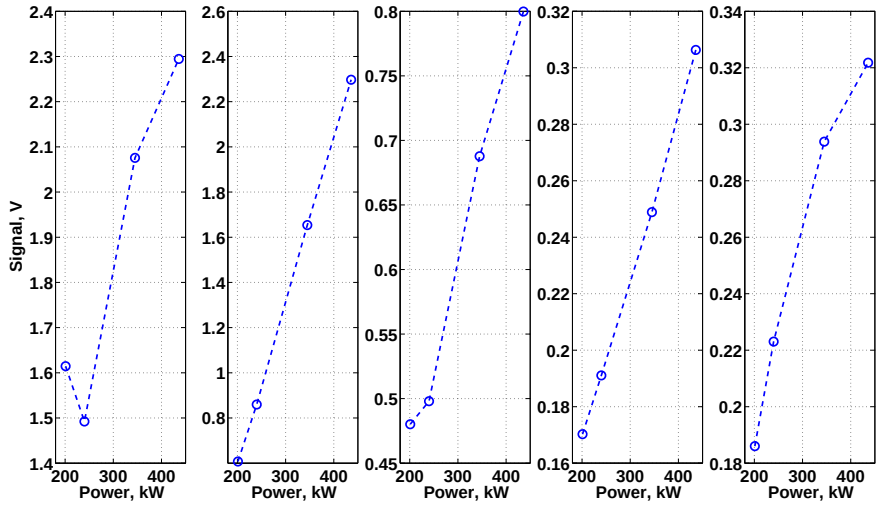

Figure 5. Raw signal of sniffer probes as a function of gyrotron power. C1 gyrotron was used as a source. From left to right: sniffer probes in modules 1-5.

that the variations in launching angles are quite small: the distance between neighboring safe launch positions is 10-15 cm.
Lastly, to increase the signal-to-noise ratio we average over 10 ms. The averaging duration is restricted by the total energy which is allowed to be injected into the vessel without plasma.

Stray radiation scales linearly with the injected microwave power. To verify our averaging procedure, we performed a power scan using the C1 gyrotron. Fig. 5 shows the readings from sniffer probes in modules 1-5, where for a single data point, signal averaging over gyrotron frequency, polarization, launch angle and time was performed as described above. We find close to linear responses of the sniffer probe voltages to increases in gyrotron power. To illustrate the importance of polarization averaging, Fig. 6 shows an example for just one polarizer angle setting. Here the polarization of the waves leads to a strongly non-linear, even non-monotonic response.

The polarization-averaged time traces of sniffer probes in modules 1-5 are shown in Fig. 7. The source of stray radiation is the C1 gyrotron in module 1.

3.3. Modeling of the ECRH stray radiation distribution

A model for describing distribution of stray radiation was presented in reference [16]. In this model, the stellarator is represented as a number of interconnected volumes - 'resonators'. Stray radiation in the model is considered isotropic, uniform, and arbitrarily polarized in each resonator. The stray radiation energy flux is determined by a power balance. Therefore, stray radiation level in resonator k can be found by solving

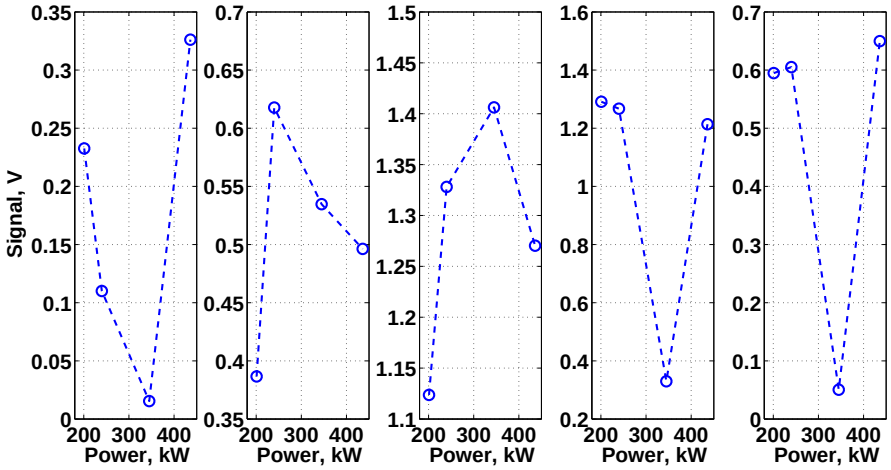

Figure 6. Raw signal of sniffer probes as a function of gyrotron power. D5 gyrotron was used as a source. Polarization averaging is not performed. From left to right: sniffer probes in modules 1-5.

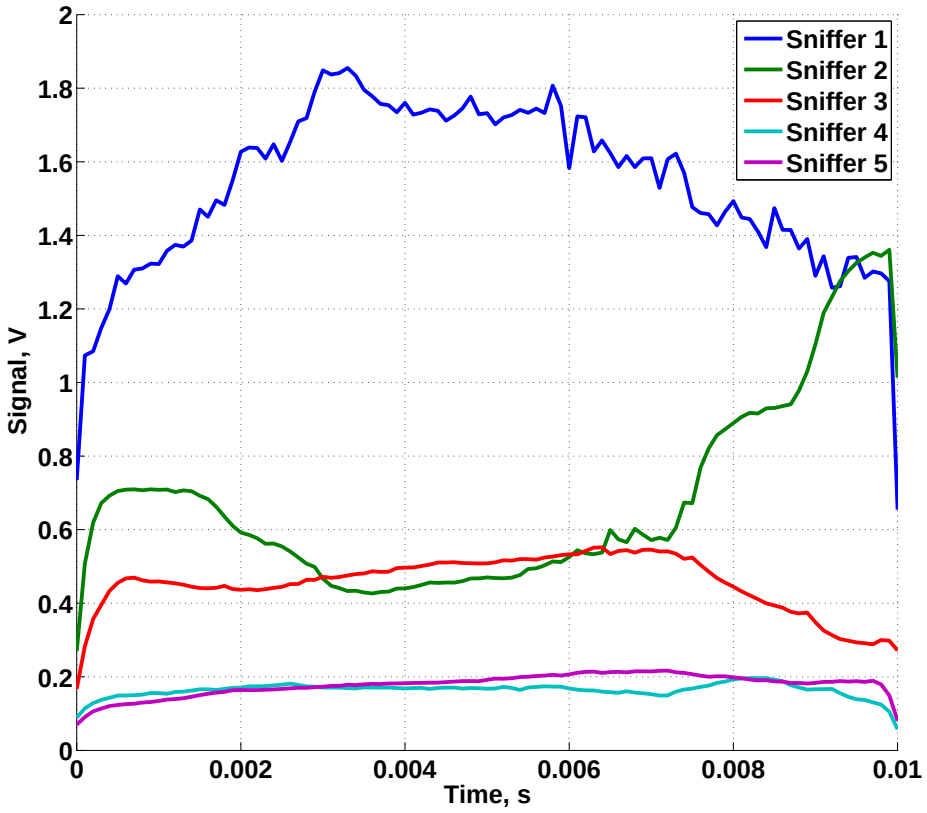

Figure 7. Average time traces from all five sniffer probes installed in modules 1-5. The gyrotron power was modulated by 90% with 10 kHz frequency.

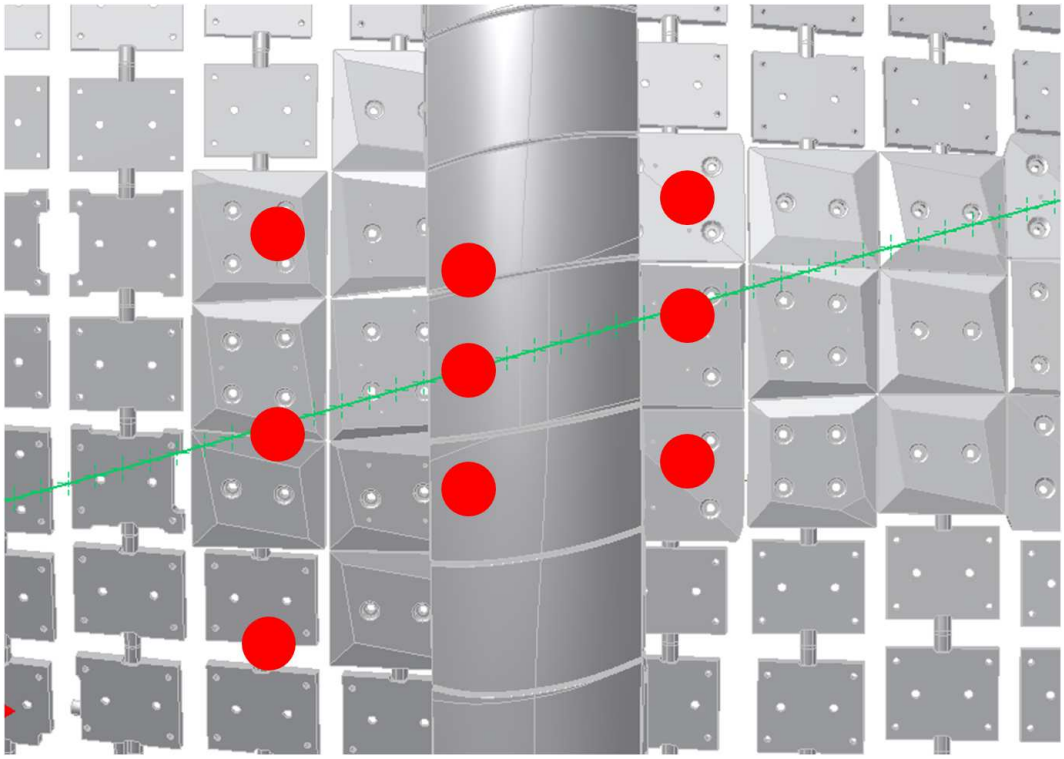

Figure 8. Beam impact positions for the D5 gyrotron on the back side of the inner wall of Wendelstein 7-X are shown as red circles. They are located partly in half-module 51 and partly in half-module 50.

Eq. (1):

$$P_{in,k} = \sum_{i=abs.surfaces} p_k A_i \eta_i + \sum_{j=interfaces} (p_k - p_j) S_{jk} \tag{1}$$

here $P_{in,k}$ (W) denotes input power in the resonator k, p_k (W/m^2) - stray radiation energy flux in the resonator k, index i runs through microwave absorbing surfaces in the resonator k, A_i (m^2) is a surface area of the absorber i, η_i is its absorption coefficient, index j runs through all other resonators in the system, p_j (W/m^2) is stray radiation energy flux in the resonator j, S_{jk} is the area of interface between current resonator k and resonator j.

A model of the Wendelstein 7-X vacuum vessel from the ComponentsDB database was taken for modeling of the stray radiation distribution. The model consists of 10 identical half-modules with the elements of heat shield. An average absorption coefficient of the vessel is chosen later during the fitting procedure.

The distribution of sources in the stray radiation model is a free parameter. In the experiments with the C1 gyrotron, the source terms were distributed in the 1:1 ratio between half-modules 10 and 11; in the experiments with the D5 gyrotron the source terms were distributed in the ratio 1:1 between half-modules 50 and 51. The reason for

such a distribution is positions and directions of the corresponding gyrotron launchers in the vacuum vessel of Wendelstein 7-X.

3.4. Forward modeling

The modeling of the C1 gyrotron experiments was performed, where the input power was scaled to 1 MW and the sniffer probe readings were scaled accordingly. The readings of the sniffer probes in modules 2 - 5 were calibrated against the modeled stray radiation energy flux in half-modules 21, 31, 41, and 51 respectively. The effective absorption area of the Wendelstein 7-X vacuum vessel $A_{eff} = A_{wall}\overline{\eta} = 5.67\ m^2$. The average microwave absorption coefficient $\overline{\eta}$ of the vacuum vessel is about 1%. The determination of the average absorption and therefore of the calibration coefficients, was done by forward modeling. The procedure of the forward modeling is presented in Fig. 9:

- An initial guess about average absorption coefficient is made.
- Simulations of two experiments where the gyrotrons C1 and D5 are used as sources of stray radiation.
- Sniffer probes 2 - 5 are calibrated against the computed stray radiation level in half-modules 21, 31, 41, 51, where they are installed, for the experiments with the C1 gyrotron as a source. No such calibration is done for sniffer probe 1 in the half-module 11 because an initial assumption of uniform and isotropic distribution of stray radiation does not hold there. There is too much of direct beam irradiation.
- Stray radiation level in modules 11, 21, 31, and 41 are computed in the simulation considering the D5 gyrotron as a source.
- Apply the obtained calibration coefficients to the sniffer probe readings from the experiments with the D5 gyrotron as a source.
- Compare measured and simulated stray radiation levels in half-modules 21, 31, and 41 in the case of the D5 gyrotron used as a source.
- Update the average microwave absorption coefficient in order to minimize the difference.

In the absolute calibration scheme shown in Fig. 9 the C1 gyrotron can be replaced by the D5 gyrotron and the D5 gyrotron replaced by the C1 gyrotron.The calibration is performed with gyrotron D5 as source of stray radiation whereas the optimization of the absorption coefficient is done with gyrotron C1 as source of stray radiation.
Both procedures resulted in very similar average absorption coefficient $\eta_{abs} = 2.6\%$ and slightly different calibration coefficients for sniffer probes. The calibration coefficients for sniffer probes 2-4 could be compared directly to each other, see Fig. 10.

The calibration coefficients for sniffer probes in modules one and five cannot be obtained simultaneously by two methods. Calibration for sniffer probe 1 can only be provided in calibration against simulations with the D5 gyrotron as a source; calibration for the sniffer probe 5 - in the case of using the C1 gyrotron as a source. The calibration

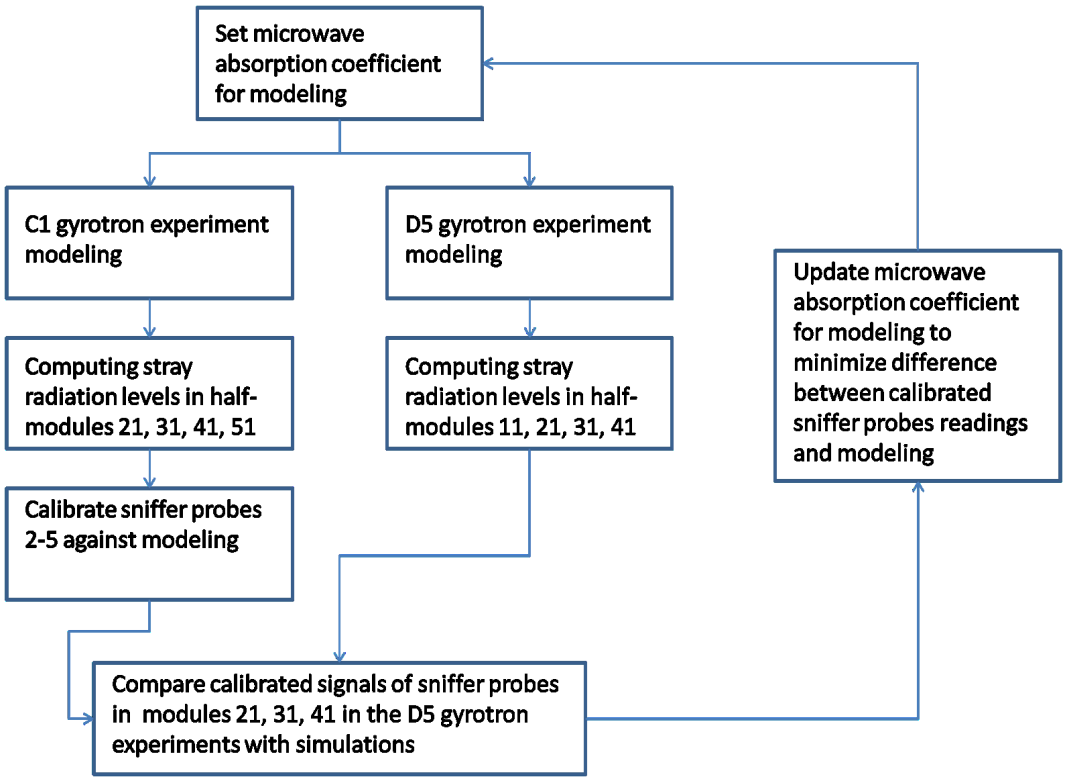

Figure 9. Schematic with the logic of sniffer probe calibration against the experiments and modeling. Here the sniffer probes are calibrated in the experiments using the C1 gyrotron as a source.

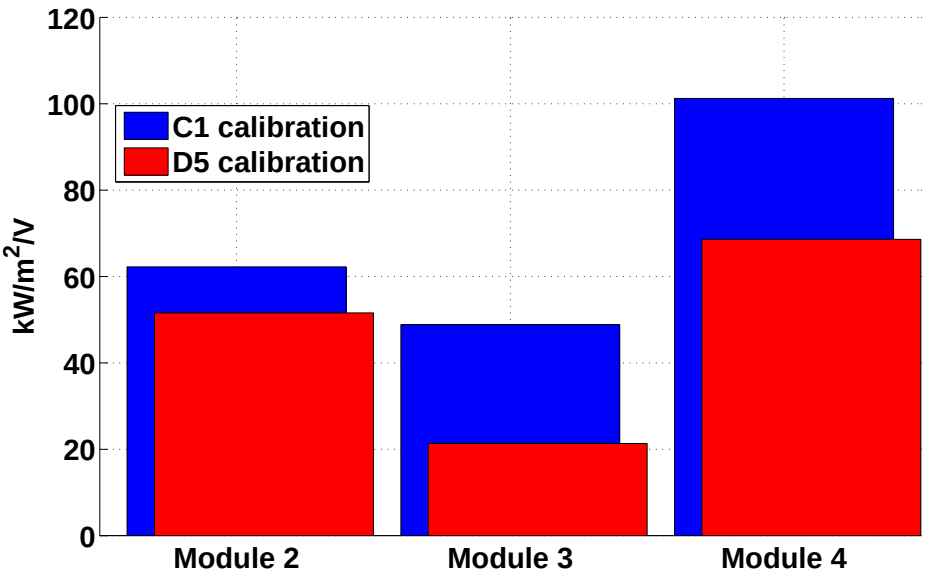

Figure 10. Comparison of absolute calibration coefficients for sniffer probes in modules 2,3, and 4. The blue bars show calibration of sniffer probes in the experiments with the C1 gyrotron as a source; the red bars show calibration of sniffer probes in the experiments with the D5 gyrotron as a source.

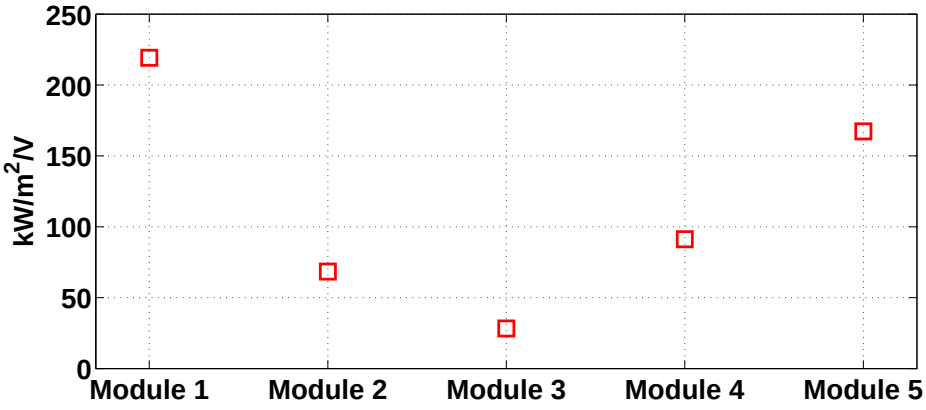

Figure 11. Calibration curve of the sniffer probes installed in modules 1-5.

coefficients for the sniffer probes in modules 2-4 are defined as mean values of the coefficients depicted in Fig. 10. The errorbars for the sniffer probes 2-4 are defined as a deviation of the calibration coefficients obtained in two different ways from their mean value:

$$\delta = \frac{abs(k_{2..4} - k_{2..4}^{C1})}{k_{2..4}} \tag{2}$$

here $k_{2..4}$ is a mean calibration coefficient for sniffer probes in modules 2-4, respectively, $k_{2..4}^{C1}$ is a calibration coefficient for sniffer probes in modules 2-4 obtained in the experiments with the C1 gyrotron as a source. Due to symmetry with respect to the mean, $k_{2..4}^{C1}$ can be replaced by $k_{2..4}^{D5}$ without changing the result.
The complete calibration curve is shown in Fig. 11

We also checked the obtained calibration to the retrospective experiments where the D5 gyrotron was used in a different regime (another accelerating voltage modulation, no polarization scan, position scan over points different to those described in Section 3). The results of the comparison of modeling of those experiment and actual measurements with calibrated sniffer probes is shown in Fig. 12. The dashed lines denote the errorbars.

After the quantification of an average absorption coefficient for the vacuum vessel, the expected levels of stray radiation during the start-up phase (without plasma) were identified. The modeling showing the case of injection from module 1 is displayed in Fig. 13 and demonstrates the stray radiation levels in the range from 80 kW/m^2 to 340 kW/m^2 per MW of input power.

4. Cross-calibration of sniffer probes

The five sniffer probes are cross-calibrated in the laboratory, so that their measurements could be compared directly. The back-end parts of sniffer probes from modules 1-5 were unmounted from the machine and cross-calibrated in the set-up shown in Fig. 15 and its schematic in Fig. 14. The front-end part of the sniffer probes is the same for all five

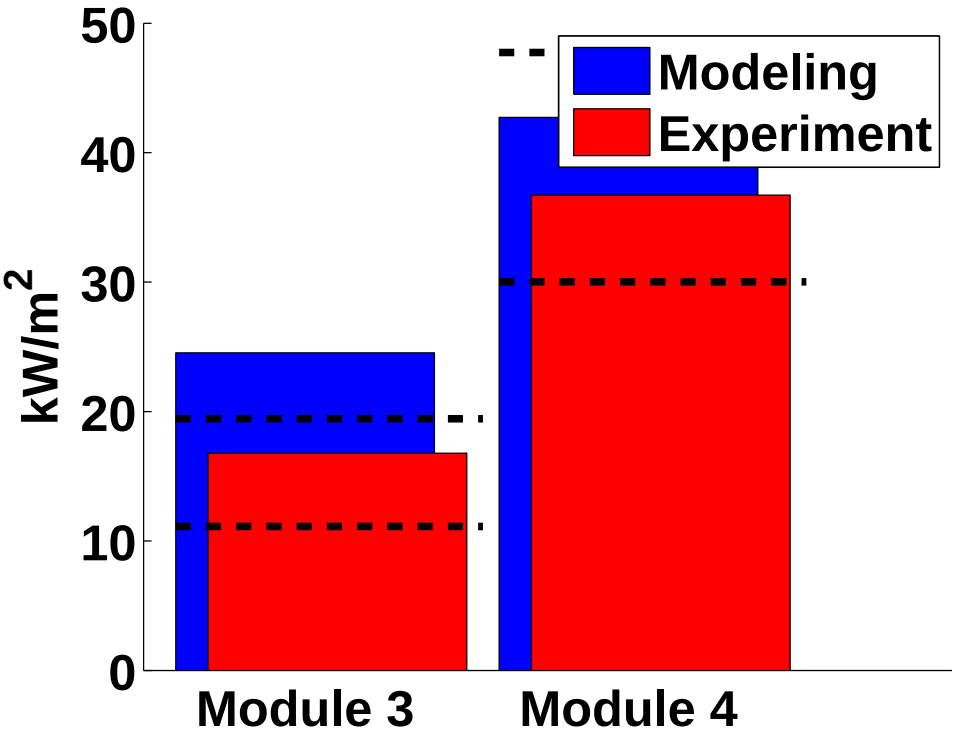

Figure 12. Comparison of calibrated sniffer probe measurements with the modeling of an independent experiment in the Wendelstein 7-X vacuum vessel with the D5 gyrotron used as a source and working in a different regime as one described in Section 3. Dashed lines show depict upper and lower errorbars.

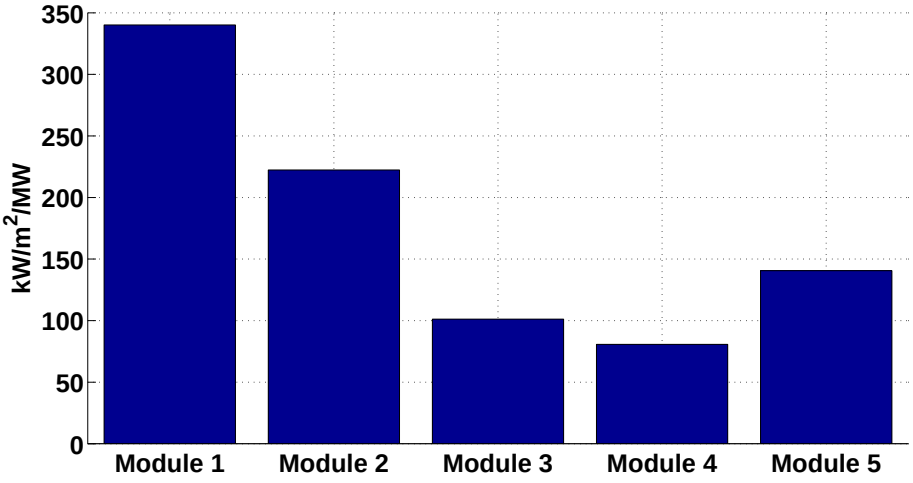

Figure 13. Stray radiation levels in the vacuum vessel of Wendelstein 7-X assuming the microwave injection from module 1. The levels range from 80 kW/m^2 to 340 kW/m^2 of stray radiation per MW of input power.

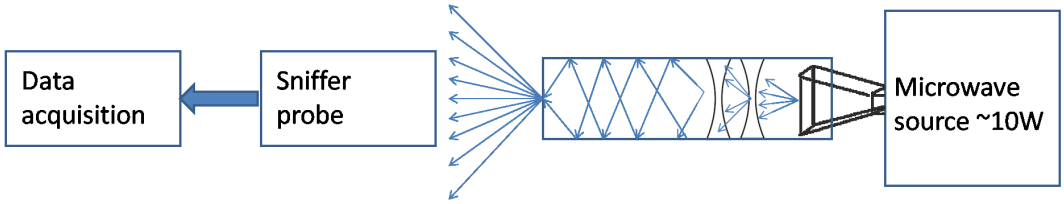

Figure 14. Schematic that illustrates how the cross-calibration experimental setup is built. The photo of the setup is shown in Fig. 15.

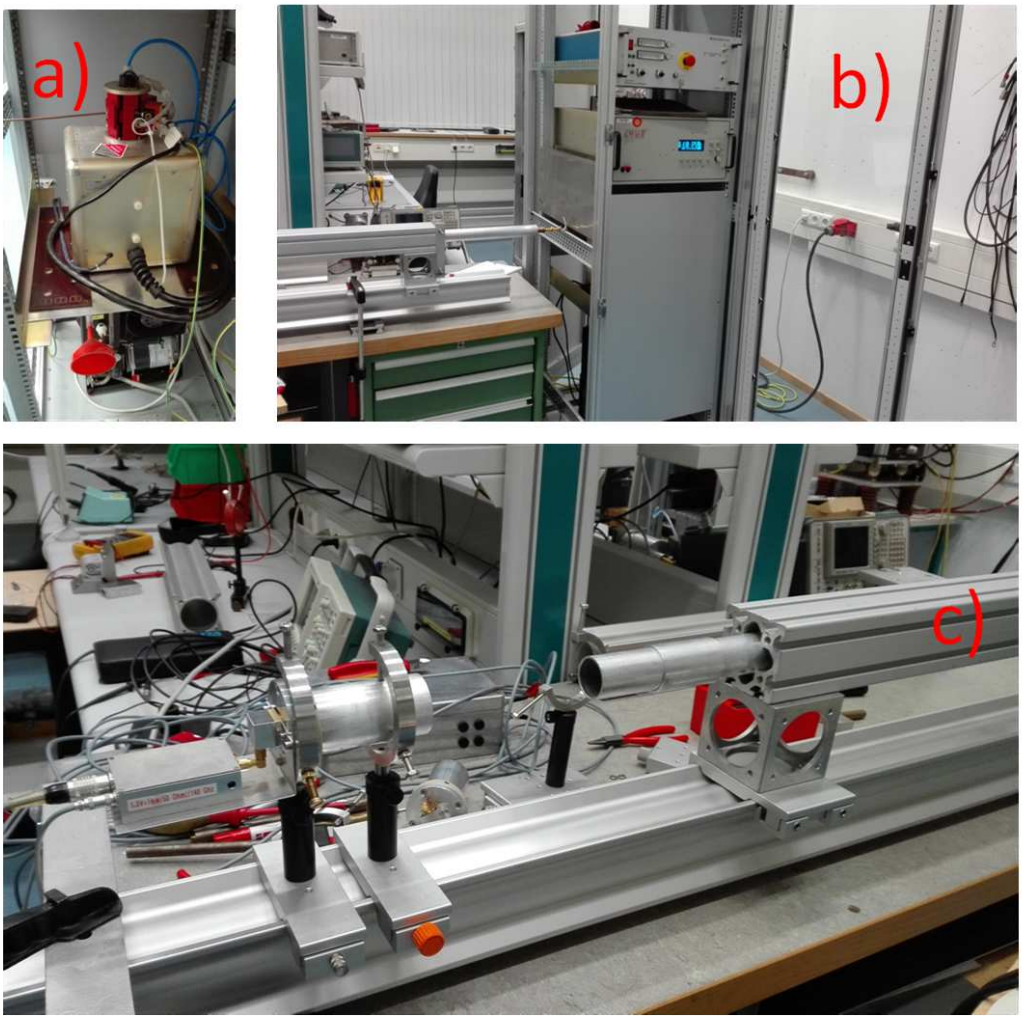

Figure 15. Photo of the cross-calibration setup. The schematic is shown in Fig. 14. (a) Microwave source, delivering approximately 10 W at 140 GHz; (b) back-end part of the cross-calibration setup, including high-voltage power supply, microwave source from panel (a), hidden behind metal sheets for security reasons, microwave antenna that emits into the oversized waveguide with built-in diverging teflon lenses; (c) front-end part of the cross-calibration setup displaying the end of the oversized waveguide and a sniffer probe on the holder.

of them and therefore have no influence on cross-calibration. The sniffer probes were irradiated in each measurement for more than 2 s, the data from the last two seconds of

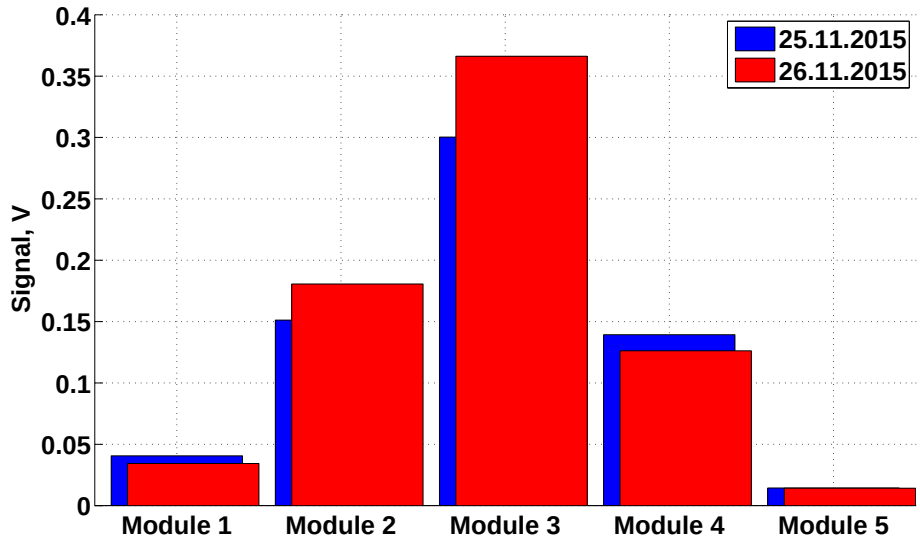

Figure 16. The average sniffer probe signals from independent experiments show the reproducibility of measurements.

acquisition was taken into analysis. Each of the sniffer probes was measured 22 times in order to average out sensitivity of microwave diodes to the polarization of microwave. In the absence of plasmas, sniffer probe measurements are known to be difficult to reproduce since the response to a single measurement is subject to particular polarization, standing wave pattern, etc. Therefore, massive amount of averaging is needed. We conducted two independent measurement sessions in order to prove the reproducibility of the measurements. The results are displayed in Fig. 16

The cross-calibration coefficients are dimensionless and are computed with respect to the sniffer probe from Module 2, see Fig. 17. The value is computed as mean value of two independent experimental sessions and the errorbars denote the discrepancy between the computed coefficients. All uncertainties are below 10%.

5. Comparison of the absolute calibration and cross-calibration of the sniffer probes

Cross-calibration and absolute calibration data can be compared when the latter is normalized to the sniffer probe calibration coefficient from module 2. The comparison is shown in Fig. 17. One can see there a good agreement between cross-calibration coefficients (blue bars) and normalized absolute calibration coefficients (red bars).
Unfortunately the sniffer probe from Module 5 was damaged during the procedure of unmounting from the machine and its microwave diode and an attenuator had to be replaced before the cross-calibration. Therefore, the data is not comparable and not presented in the Fig. 17.
The normalization of the absolute calibration coefficients was done with respect to the

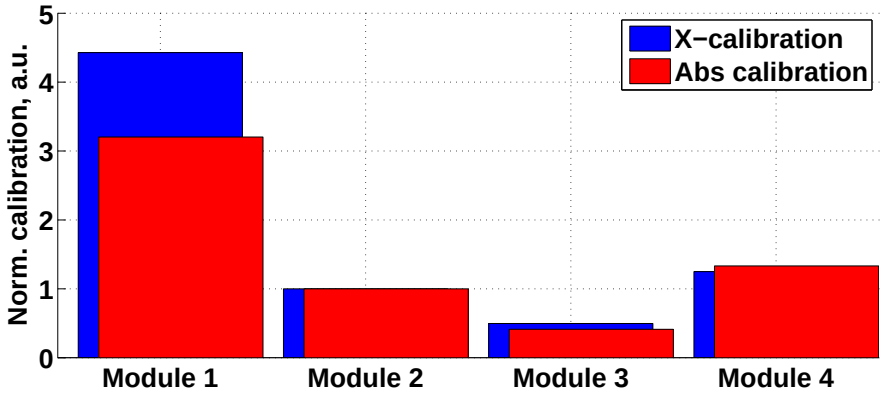

Figure 17. Comparison of cross-calibration (blue bars) and absolute calibration coefficients (red bars) of the sniffer probes. All values are shown with respect to the calibration coefficient of the sniffer probe 2. The sniffer probe from Module 5 is excluded from the analysis.

coefficient for sniffer probe 2, because it has the lowest errorbar.

For the combined calibration coefficient, the normalized shape was taken from the cross-calibration measurements. The scaling factor is the absolute calibration coefficient of sniffer probe 2, computed in Section 3. Errorbars are estimated in the following way:

$$\delta_{combined,i} = \sqrt{\delta^2_{abscalib,2} + \delta^2_{xcalib,i}}, \tag{3}$$

where $\delta_{combined,i}$ is an errorbar on combined calibration coefficient for sniffer probe i, $\delta_{abscalib,2}$ is an errorbar on the absolute calibration coefficient for sniffer probe 2, and $\delta_{xcalib,i}$ is an errorbar on the cross-calibration coefficient for sniffer probe i.

The combined normalized calibration coefficients can be scaled back to their absolute values, as shown in Fig. 18.

6. Conclusions

In this paper we present a systematic approach to calibrate sniffer probes. The extremely volatility of sniffer probe signals was overcome by averaging over time, frequency chirp, and polarization or launching direction.

The stray radiation model was validated in the Wendelstein 7-X vacuum vessel and was used for the absolute calibration of the sniffer probes. The calibration method is based on implicit estimation of the Q factor of the vacuum vessel of Wendelstein 7-X with calibrated sources. The method allows absolute calibration of sniffer probes or any other diagnostic that measure stray radiation, i.e. microwave bolometers. Independently, cross-calibration was performed and the normalized absolute calibration coefficients were compared to the cross-calibration coefficients. Both methods show good agreement. The obtained calibration coefficients were applied retrospectively to the experiment in the vessel with the D5 gyrotron as a source, working in a different regime than

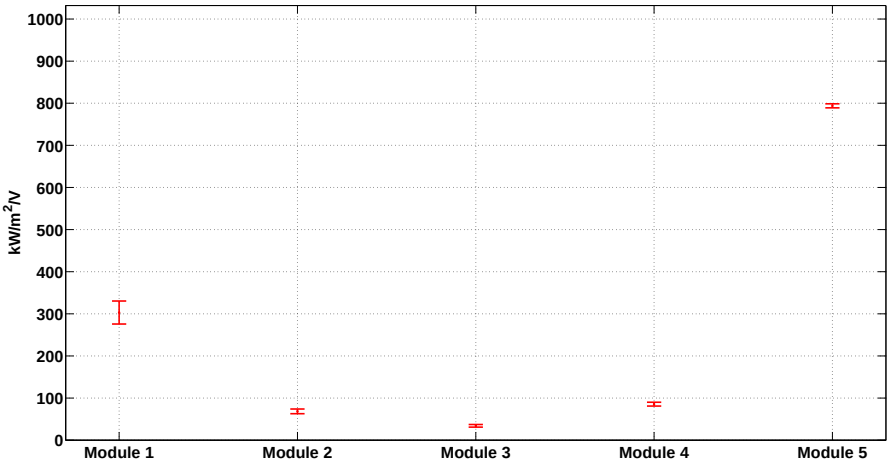

Figure 18. Combined normalized calibration coefficients for sniffer probes from modules 1-4 and their errorbars scaled to the absolute values.

discussed in the paper. The measurements show good agreement with the modeling of the experiment.

The distribution of stray radiation in the modules of Wendelstein 7-X was conducted using computed average absorption coefficient for the vacuum vessel. This distribution assumes no plasma and the C1 gyrotron as a source. These conditions are typical for the start-up phase of the stellarator. The stray radiation energy flux ranges from 340 kW/m^2 per MW of input power in module 1 (where the source is placed) to 80 kW/m^2 per MW of input power in module 3, the most remote module from the source.

Acknowledgments

Authors would like to express their gratitude and appreciation to Dr. Mirko Salewski for fruitful discussions and proof reading.

The authors are grateful to the Wendelstein 7-X team for its continuous support.

This work has been carried out within the framework of the EUROfusion Consortium and has received funding from the Euratom research and training programme 2014-2018 under grant agreement No 633053. The views and opinions expressed herein do not necessarily reflect those of the European Commission.

References

[1] M Wanner, V Erckmann, J.-H Feist, W Gardebrecht, D Hartmann, R Krampitz, H Niedermeyer, H Renner, Th Rummel, F Schauer, L Wegener, F Wesner, G.A M ller, W Kasparek, M Thumm, and G Dammertz. Status of WENDELSTEIN 7-X construction. *Nuclear Fusion*, 43(6):416–424, June 2003.

[2] V. Erckmann, P. Brand, H. Braune, G. Dammertz, G. Gantenbein, W. Kasparek, H. P. Laqua, H. Maassberg, N. B. Marushchenko, G. Michel, M. Thumm, Y. Turkin, M. Weissgerber, and

A. Weller. Electron Cyclotron Heating for W7-X: Physics and Technology. *Fusion Science and Technology*, 52(2):291–312, August 2007.

[3] V. Erckmann, P. Brand, H. Braune, G. Dammertz, G. Gantenbein, W. Kasparek, H. P. Laqua, G. Michel, M. Thumm, and M. Weissgerber. The 140 GHz, 10 MW, CW ECRH Plant for W7-X: A Training Field for ITER. In *Fusion Energy 2006*, pages IT/2–4Rd, Chengdu, 2007. International Atomic Energy Agency.

[4] J Geiger, R C Wolf, C Beidler, A Cardella, E Chlechowitz, V Erckmann, G Gantenbein, D Hathiramani, M Hirsch, W Kasparek, J Kiß linger, R König, P Kornejew, H P Laqua, C Lechte, J Lore, A Lumsdaine, H Maaß berg, N B Marushchenko, G Michel, M Otte, A Peacock, T Sunn Pedersen, M Thumm, Y Turkin, A Werner, and D Zhang. Aspects of steady-state operation of the Wendelstein 7-X stellarator. *Plasma Physics and Controlled Fusion*, 55(1):014006, January 2013.

[5] H J Hartfuss, V Erckmann, M Hirsch, and H Laqua. Problems with ECRH stray radiation in Wendelstein 7-X. In *28th EPS Conference on Contr. Fusion and Plasma Phys.*, volume 27, pages O–3.2C, St. Petersburg, Russia, 2003.

[6] D Moseev, F Meo, S B Korsholm, T Koskela, M Albergante, O Asunta, H Bindslev, A Bürger, V Furtula, M Kantor, F Leipold, P K Michelsen, S K Nielsen, M Salewski, O Schmitz, M Stejner, and E Westerhof. Comparison of measured and simulated fast ion velocity distributions in the TEXTOR tokamak. *Plasma Physics and Controlled Fusion*, 53(10):105004, 2011.

[7] M Nishiura, S Kubo, K Tanaka, N Tamura, T Shimozuma, T Mutoh, K Kawahata, T Watari, T Saito, Y Tatematsu, and T Notake. Initial result of collective Thomson scattering using 77 GHz gyrotron for bulk and tail ion diagnostics in the Large Helical Device. *Journal of Physics: Conference Series*, 227:012014, May 2010.

[8] M Salewski, F Meo, M Stejner, O Asunta, H Bindslev, V Furtula, S B Korsholm, T Kurki-Suonio, F Leipold, F Leuterer, P K Michelsen, D Moseev, S K Nielsen, J Stober, G Tardini, D Wagner, and P Woskov. Comparison of fast ion collective Thomson scattering measurements at ASDEX Upgrade with numerical simulations. *Nuclear Fusion*, 50(3):035012, March 2010.

[9] M Salewski, S K Nielsen, H Bindslev, V Furtula, N N Gorelenkov, S B Korsholm, F Leipold, F Meo, P K Michelsen, D Moseev, and M Stejner. On velocity space interrogation regions of fast-ion collective Thomson scattering at ITER. *Nuclear Fusion*, 51(8):083014, 2011.

[10] Ralf König, J. Baldzuhn, W. Biel, C. Biedermann, H.S. Bosch, S. Bozhenkov, T. Bräuer, B. Brotas de Carvalho, R. Burhenn, B. Buttenschön, G. Cseh, A. Czarnecka, M. Endler, V. Erckmann, T. Estrada, J. Geiger, O. Grulke, D. Hartmann, D. Hathiramani, M. Hirsch, S. Jabonski, M. Jakubowski, J. Kaczmarczyk, T. Klinger, S. Klose, G. Kocsis, P. Kornejew, A. Krämer-Flecken, T. Kremeyer, M. Krychowiak, M. Kubkowska, A. Langenberg, H. P. Laqua, M. Laux, Y. Liang, A. Lorenz, A.O. Marchuk, V. Moncada, O. Neubauer, U. Neuner, J.W. Oosterbeek, M. Otte, N. Pablant, E. Pasch, T.S. Pedersen, K. Rahbarnia, L. Ryc, O. Schmitz, W. Schneider, H. Schuhmacher, B. Schweer, T. Stange, H. Thomsen, J.-M. Travere, T. Szepesi, U. Wenzel, A. Werner, B. Wiegel, T. Windisch, R. Wolf, G.A. Wurden, D. Zhang, A. Zimbal, S. Zoletnik, and the W7-X Team. The Set of Diagnostics for the First Operation Campaign of the Wendelstein 7-X Stellarator, October 2015.

[11] M. Preynas, H. P. Laqua, S. Marsen, A. Reintrog, Y. Corre, V. Moncada, and J.-M. Travere. A near infra-red video system as a protective diagnostic for electron cyclotron resonance heating operation in the Wendelstein 7-X stellarator. *Review of Scientific Instruments*, 86(11):113504, November 2015.

[12] F Gandini, S Cirant, M Hirsch, H.P Laqua, S Nowak, A Bruschi, G Granucci, V Erckmann, V Mellera, V Muzzini, A Nardone, A Simonetto, C Sozzi, and N Spinicchia. The detection of the non-absorbed millimeterwave power during EC heating and current drive. *Fusion Engineering and Design*, 56-57:975–979, October 2001.

[13] Martin Schubert, Albrecht Herrmann, Francesco Monaco, Volker Rohde, Harald Schütz, Jörg Stober, Thomas Vierle, Stefan Vorbrugg, Dietmar Wagner, Dieter Zasche, Thomas Zehetbauer,

and Wolfgang Zeidner. Machine safety issues with respect to the extension of ECRH systems at ASDEX Upgrade. *EPJ Web of Conferences*, 87:02010, March 2015.

[14] H. Igami, S. Kubo, H. P. Laqua, K. Nagasaki, S. Inagaki, T. Notake, T. Shimozuma, Y. Yoshimura, and T. Mutoh. Searching for O-X-B mode-conversion window with monitoring of stray microwave radiation in LHD. *Review of Scientific Instruments*, 77(10):10E931, October 2006.

[15] Shen Baoli, Ren Wu, Gao Benqing, and Yang Shiming. The analysis of several diffusers in a reverberation chamber by FDTD method. In *2002 3rd International Conference on Microwave and Millimeter Wave Technology, 2002. Proceedings. ICMMT 2002.*, pages 911–914. IEEE, 2002.

[16] H P Laqua, V Erckmann, and M Hirsch. Distribution of the ECRH stray radiation in fusion devices. In *28th EPS Conference on Contr. Fusion and Plasma Phys.*, number June, page P3.099, 2001.